



The JCMT Transient Survey: An Extraordinary Submillimeter Flare in the T Tauri Binary System JW 566

Steve Mairs¹, Bhavana Lalchand², Geoffrey C. Bower³, Jan Forbrich⁴, Graham S. Bell¹, Gregory J. Herczeg⁵,
Doug Johnstone^{6,7}, Wen-Ping Chen², Jeong-Eun Lee⁸, and Alvaro Hacar⁹

¹East Asian Observatory, 660 N. A'ohoku Place, Hilo, HI 96720, USA; s.mairs@eaobservatory.org

²Graduate Institute of Astronomy, National Central University, 300 Zhongda Road, Zhongli, Taoyuan 32001, Taiwan

³Academia Sinica Institute of Astronomy and Astrophysics, 645 N A'ohoku Place, Hilo, HI 96720, USA

⁴Centre for Astrophysics Research, School of Physics, Astronomy and Mathematics, University of Hertfordshire, College Lane, Hatfield AL10 9AB, UK

⁵Kavli Institute for Astronomy and Astrophysics, Peking University, Yiheyuan Lu 5, Haidian Qu, 100871 Beijing, Peoples Republic of China

⁶NRC Herzberg Astronomy and Astrophysics, 5071 West Saanich Road, Victoria, BC, V9E 2E7, Canada

⁷Department of Physics and Astronomy, University of Victoria, Victoria, BC, V8P 5C2, Canada

⁸School of Space Research, Kyung Hee University, 1732, Deogyong-Daero, Giheung-gu Yongin-shi, Gyunggi-do 17104, Republic of Korea

⁹Leiden Observatory, Leiden University, P.O. Box 9513, 2300-RA Leiden, The Netherlands

Received 2018 August 31; revised 2018 November 23; accepted 2018 November 24; published 2019 January 23

Abstract

The binary T Tauri system JW 566 in the Orion Molecular Cloud underwent an energetic, short-lived flare observed at submillimeter wavelengths by the SCUBA-2 instrument on 2016 November 26 (UT). The emission faded by nearly 50% during the 31 minute integration. The simultaneous source fluxes averaged over the observation are 500 ± 107 mJy beam⁻¹ at 450 μ m and 466 ± 47 mJy beam⁻¹ at 850 μ m. The 850 μ m flux corresponds to a radio luminosity of $L_\nu = 8 \times 10^{19}$ erg s⁻¹ Hz⁻¹, approximately one order of magnitude brighter (in terms of νL_ν) than that of a flare of the young star GMR-A, detected in Orion in 2003 at 3mm. The event may be the most luminous known flare associated with a young stellar object and is also the first coronal flare discovered at submillimeter wavelengths. The spectral index between 450 and 850 μ m of $\alpha = 0.11$ is broadly consistent with nonthermal emission. The brightness temperature was in excess of 6×10^4 K. We interpret this event to be a magnetic reconnection that energized charged particles to emit gyrosynchrotron/synchrotron radiation.

Key words: ISM: jets and outflows – stars: formation – stars: variables: general – surveys

1. Introduction

Young stellar objects (YSOs) host a range of high-energy phenomena, pointing toward magnetic activity (e.g., Feigelson & Montmerle 1999; Benz & Güdel 2010). Of the variability of YSOs across the electromagnetic spectrum, radio and X-ray variability are most closely related to magnetic activity, and indeed YSOs show strong, very short lived flares in these wavelength ranges. X-ray flares of this nature have been comparatively well-studied (e.g., Getman et al. 2008a, 2008b), whereas observations of greater numbers of nonthermal radio flares on timescales of hours or less have only recently become possible with sensitivity improvements, and thus comparably few sources such as these are known at this time. So far, the majority of observations of radio variability have been made on timescales of \sim days to years.

The first example of a YSO radio flare was reported by Bower et al. (2003) toward the weak-line T Tauri star (class III YSO) GMR-A. The flux density at an observing frequency of 86 GHz rose by more than a factor of 5 within a few hours. X-ray monitoring of the source also revealed contemporaneous activity. Follow-up millimeter observations were performed by Furuya et al. (2003), who observed subsequent flare activity for \sim two weeks. Another strong flare at an observing frequency of 90 GHz was reported by Massi et al. (2006) toward the weak-line T Tauri star V773 Tau, which also happened to be the first case with evidence for interbinary magnetic interaction. Salter et al. (2008) observed a 3 mm flare associated with the DQ Tau and showed evidence that these events may be expected for similar binary systems. Even the earliest evolutionary stages of

a forming star show activity: Forbrich et al. (2008) reported a strong flare at 22 GHz toward a very deeply embedded protostar in the Orion BN/KL region. In all of these cases, the radio emission is interpreted as nonthermal radiation.

Giant flares from young stars are important both for understanding magnetic reconnection as well as for evaluating the impact of high-energy photons on protoplanetary disks and atmospheric escape (e.g., Güdel et al. 2014). The X-ray emission from flares, produced by hotter gas than quiescent X-ray emission, emits energetic photons that penetrate deep into the disk (Glassgold et al. 2004), thereby affecting midplane ionization and chemistry (e.g., Rab et al. 2017; Fraschetti et al. 2018). Variability has been detected in H¹³CO⁺ emission and attributed to flares (Cleeves et al. 2017). Flash-heating from X-rays is a possible explanation for producing chondrites (Shu et al. 1997) and abundances of calcium-rich inclusions seen in meteorites (Sossi et al. 2017). Once planets form, the ultraviolet and X-ray emission and cosmic rays produced by magnetic reconnection affects the atmospheric chemistry and enhances their escape (e.g., Lammer et al. 2018).

The correlation between X-ray and radio variability in YSOs has remained unclear, however, even though there is undoubtedly an underlying connection (e.g., Güdel & Benz 1993). Recently, Forbrich et al. (2016, 2017) analyzed the incidence of order-of-magnitude flaring variability on short timescales in the Orion Nebula Cluster, using simultaneous radio (4.7 and 7.3 GHz) and X-ray observations. They found that there is a close connection only for a subset of this extreme radio and X-ray variability.

In this paper, we present the detection of a submillimeter-wavelength outburst from the YSO JW 566 in Orion, discovered in the James Clerk Maxwell telescope (JCMT)-Transient submillimeter monitoring program of nearby star-forming regions (Herczeg et al. 2017). This flare falls into the same category as the short timescale, likely nonthermal radio flares described above. The short timescale for the decay of the flare rules out reprocessed accretion luminosity through thermal dust emission in the envelope (Johnstone et al. 2013) as the source of variability, which until this paper had been the type of variability uncovered within our survey (Mairs et al. 2017a; Yoo et al. 2017; Johnstone et al. 2018), even though this observation by itself does not necessarily imply entirely distinct emission mechanisms. This is the first such flare discovered at submillimeter wavelengths. In Section 2, we present details of our observations and data reduction methods. In Section 3, we introduce the methods used to detect the flare. In Section 4, we display the 450 and 850 μm images and construct a short timescale light curve of the flare. In Section 5, we discuss the results and compare the data presented in this paper to previous observations of JW 566 at other wavelengths. Finally, in Section 6, we summarize our findings.

2. Observations and Data Reduction

2.1. SCUBA-2 Observations

The JCMT Transient Survey (project code: M16AL001; Herczeg et al. 2017) has been monitoring submillimeter emission from the Orion Molecular Cloud (OMC) 2/3 region, centered at (R.A., decl.) = (05:35:33, $-5:00:32$, J2000), and seven other nearby star-forming regions with a roughly monthly cadence since 2015 December. Each region is observed with SCUBA-2 (Holland et al. 2013) at 450 and 850 μm simultaneously, with beam sizes of $9''.8$ and $14''.6$, respectively (Dempsey et al. 2013). The images are constructed using $2''$ pixels at 450 μm and $3''$ pixels at 850 μm . The SCUBA-2 observing mode *Pong1800* (Kackley et al. 2010) yields maps with a smooth sensitivity over a circular region with $30'$ diameter. Our integration times are set to ensure a consistent background noise level of ~ 10 mJy beam $^{-1}$ at 850 μm from epoch to epoch (Mairs et al. 2017b). At 450 μm , the submillimeter emission from the atmosphere has a much more significant effect on the data, producing a range of noise levels that span more than an order of magnitude.

Table 1 provides a log for our observations of OMC 2/3. The flare is detected in our observations of 2016 November 26, beginning at MJD = 57718.453 and ending at MJD = 57718.474. We also include in our analysis of JW 566 engineering/commissioning observations (project code M16BEC30) obtained on 2016 November 20 (UT), 6 days before the flare, which were obtained to assess the health of SCUBA-2 after maintenance. This engineering observation is used only to determine the detectability of JW 566, and is excluded from our coadded images and global analysis.

2.2. Data Reduction and Flux Uncertainties

The data reduction was carried out using the iterative map-making software, MAKEMAP (see Chapin et al. 2013 for details), which is part of STARLINK's (Currie et al. 2014) Submillimetre User Reduction Facility (SMURF) package (Jenness et al. 2013). The specific data reduction and image calibration techniques used by the JCMT Transient Survey are

Table 1
A Summary of the OMC 2/3 Observations^a Performed by the JCMT Transient Survey to Date

| UT Date (YYYY-MM-DD) | Scan ^b | τ_{225} ^c | Airmass | 850 μm σ_{rms} ^d (mJy beam $^{-1}$) | 450 μm σ_{rms} ^d (mJy beam $^{-1}$) |
|--------------------------|-------------------|---------------------------|-------------|---|---|
| 2015 Dec 26 | 36 | 0.11 | 1.13 | 9.9 | 411.2 |
| 2016 Jan 16 | 19 | 0.06 | 1.21 | 7.7 | 81.3 |
| 2016 Feb 06 | 12 | 0.04 | 1.36 | 9.7 | 73.4 |
| 2016 Feb 29 | 11 | 0.04 | 1.16 | 9.4 | 67.4 |
| 2016 Mar 25 | 15 | 0.06 | 1.27 | 8.7 | 101.8 |
| 2016 Apr 22 | 11 | 0.05 | 1.72 | 9.1 | 126.4 |
| 2016 Aug 26 | 20 | 0.11 | 1.26 | 12.1 | 398.6 |
| 2016 Nov 20 ^e | 20 | 0.084 | 1.31 | 7.9 | 174.8 |
| 2016 Nov 26 | 52 | 0.06 | 1.11 | 7.7 | 85.2 |
| 2017 Feb 06 | 21 | 0.12 | 1.15 | 9.8 | 392.5 |
| 2017 Mar 18 | 12 | 0.10 | 1.10 | 9.1 | 255.6 |
| 2017 Apr 21 | 22 | 0.09 | 1.41 | 10.4 | 382.8 |
| 2017 Jul 08 | 73 | 0.05 | 1.24 | 9.4 | 72.1 |
| 2017 Aug 12 | 56 | 0.07 | 1.60 | 8.5 | 187.1 |
| 2017 Sep 12 | 54 | 0.10 | 1.32 | 9.0 | 280.3 |
| 2017 Oct 21 | 47 | 0.09 | 1.11 | 8.0 | 164.8 |
| 2017 Nov 18 | 46 | 0.06 | 1.10 | 9.5 | 77.6 |
| 2017 Dec 24 | 46 | 0.07 | 1.36 | 8.5 | 148.5 |
| 2018 Feb 08 | 18 | 0.09 | 1.20 | 8.0 | 184.6 |
| 2018 Mar 08 | 15 | 0.11 | 1.64 | 10.4 | 780.1 |

Notes. Bold text highlights the date of the flare event (see Section 5).

^a The target identifier in the JCMT archive is OMC2-3.

^b The observation number.

^c τ_{225} is the zenith opacity of the atmosphere at 225 GHz.

^d Noise measurements are based on the pixel variances in a central $900''$ radius of the Gaussian smoothed map.

^e This data was taken as part of an engineering and commissioning project (project ID: M16BEC30) and not as part of the JCMT Transient Survey.

described in detail by Mairs et al. (2017b; reduction R3 with no relative flux calibration applied¹⁰). Briefly, to perform a *Pong1800* observation, the telescope continually scans across the sky, observing each location at a variety of position angles. This technique allows for the modeling and subtraction of the large-scale, bright, variable atmosphere at submillimeter wavelengths. The continual scanning across the sky also provides a time-series that is exploited in this paper to measure light curves during our observation.

To optimize the extraction of compact sources, we applied a stringent spatial filter during the data reduction to suppress the signal on scales $>200''$. A mask was used to define significant astronomical emission in the image, which provided additional constraints to MAKEMAP and aided in the background subtraction (see Chapin et al. 2013; Mairs et al. 2015). The OMC 2/3 region is particularly difficult to mask due to the large amount of extended emission, though all persistent point sources are well accounted for in the regular analysis pipeline. The source with a strong flare, JW 566, resides in a region of negative bowing, a section of the image with artificially low values just outside the boundaries of bright, extended emission, due to the application of the stringent spatial filter. The external mask was therefore adjusted to include the bright event

¹⁰ To suppress the false detections of noise spikes or artificial structure, the images are smoothed with Gaussian kernels with FWHM values of $4''$ and $6''$ at 450 μm and 850 μm , respectively (two pixels in each case).

associated with JW 566 and the data reduction was rerun for all epochs to ensure the flux of the source was well recovered.

In addition, all Transient Survey epochs, excluding 2016 November 26 (the date of the flare event), were then coadded and subtracted from the 2016 November 26 data to produce residual flux maps at 450 and 850 μm . The fluxes of JW 566 quoted in Section 4 were measured in the residual maps to suppress any background structure present in the image. At 850 μm , the background level of the coadd at the location of JW 566 is 2 mJy beam⁻¹, which is insignificant relative to the peak flux measurement of the source. We adopt the JCMT standard flux uncertainty value of 10% for 850 μm observations (Dempsey et al. 2013; S. Mairs et al. 2018, in preparation). At 450 μm , however, JW 566 is located within a negative bowl in the coadded image, with a background level of -100 mJy beam⁻¹. The standard deviation of the mean negative bowl depth within the region of JW 566 for observations with similar background noise (450 μm $\sigma_{\text{rms}} < 120$ mJy beam⁻¹) is 77 mJy beam⁻¹ (see Table 1). We therefore combine the JCMT standard flux uncertainty value at 450 μm of 15% (Dempsey et al. 2013; S. Mairs et al. 2018, in preparation) with the uncertainty in the negative bowl depth for an uncertainty of 21% for JW 566.

The fluxes described in this paper ignore any emission from ¹²CO J = 3–2, which is located within the 850 μm filter of SCUBA-2 (for a discussion on the effects of CO contamination, see Drabek et al. 2012; Coudé et al. 2016; Parsons et al. 2018). In the JCMT Gould Belt Survey image of ¹²CO emission obtained with the Heterodyne Array Receiver Programme (HARP) (Buckle et al. 2009), weak CO emission is dispersed across the location of JW 566 with no significant compact structure, and has a negligible effect on the continuum emission described in this paper.

2.3. Subdividing the Raw Data

Raw SCUBA-2 data are comprised of the power received at the focal plane over time, with separate integrations read out and saved in ~ 36 s intervals, some of which include observations of JW 566. In Section 4.3, we subdivide this data stream into nine shorter integrations based on when the telescope passed over JW 566. These subdivisions are reconstructed into individual images using the same external mask and data reduction parameters as for the full integration.

3. Searching for Variability of Faint Sources

At the time of writing, the JCMT Transient Survey has obtained nearly 3 yr of data across eight star-forming regions. Johnstone et al. (2018) analyzed source variability in all 850 μm images taken throughout the first 18 months of the survey (2015 December through 2017 May). The 1643 sources in that analysis were selected by identifying compact emission peaks with a brightness five times higher than the noise in the coadded maps of each region in our survey. Since that time, these same sources have been tracked with an automated pipeline that measures the flux soon after the data are obtained and compares it with past observations. The automated version of the Johnstone et al. (2018) analysis, however, relies on the initial detection of a source in the coadded image of a given target field. Therefore, the pipeline is only sensitive to short timescale burst events that are strong enough to be detected at a level of $5\sigma_{\text{rms}}$ in the coadd. We are now in the process of further

evaluating transient variability by searching for any sources that might have appeared in only a single image (B. Lalchand et al. 2018, in preparation). Following the methods of Johnstone et al. (2018), we use the JSA_CATALOGUE program (found in STARLINK’s PICARD package Gibb et al. 2013) to optimize and run the FELLWALKER (Berry 2015) source detection algorithm to identify compact, peaked, continuum emission structures. While Johnstone et al. (2018) used this strategy to produce a source catalog from the coadded image of a field, we repeat their procedure for each individual epoch in the OMC 2/3 region. In this way, we compare the catalogs generated for each epoch with the catalog generated for the coadd and identify sources that appeared in individual observations, but not in the averaged image. We refer to these sources as candidate transients.

Figure 1 shows the 850 μm source peak (the maximum pixel value in each source footprint) of all the sources detected in the OMC 2/3 coadd (gray) versus the effective diameter. The effective diameter of a source is calculated by measuring the total area in the identified clump footprint and assuming a projected circular symmetry. Since this method takes into account the full clump size (and not the brightness profile), unresolved sources will appear larger than the beam FWHM, while false detections due to residual correlated noise in the final image will appear smaller than the beam FWHM. The circular symmetry assumption holds well for compact (approximately beam-sized) objects. Also included (green) are the sources detected only in individual epochs. Several faint, spurious sources that do not appear at the level of $5\sigma_{\text{rms}}$ in the coadd and are smaller than the beam are detected in single epochs. A full, multiregion analysis of candidate transients like these will be presented by B. Lalchand et al. (2018, in preparation).

One unresolved¹¹ source, however, is a clear outlier. This source is detected at (R.A., decl.) = (5:35:17.94, $-5:16:11$) on 2016 November 26 (UT), with an initial 850 μm source peak of 384 mJy beam⁻¹ in an observation that had a background noise level of $\sigma_{\text{rms}} = 9.74$ mJy beam⁻¹ (S/N = 39). This flux, however, is underestimated as it was measured before the image was rereduced with an appropriate mask (see Section 2.2). The 2016 November 26 epoch is the only image with a detection of this source. The source was not identified in our initial measurements of variability from the first 11 epochs of the survey (Johnstone et al. 2018) because negative bowling in the region of JW 566 led to an average source brightness of ~ 0.8 mJy beam⁻¹ at the peak pixel location.

The position of this candidate transient peak is within $2''.4$ of the position of JW 566 (Jones & Walker 1988), a K7+M1.5 T Tauri binary system with a projected separation of $0''.86$ (Daemgen et al. 2012). It has been classified as a “Disk” by Megeath et al. (2012) based on its midinfrared colors.

4. A Submillimeter Flare of JW 566

4.1. Detecting the Flare at 850 μm

Out of 20 epochs of SCUBA-2 imaging, only one (2016 November 26) shows bright, unresolved 850 μm emission at the location of JW 566 (see Table 1 and Figure 2). Figure 2

¹¹ A Gaussian fit at the position of the significant candidate transient source in the smoothed, 850 μm image results in a full width at half maximum value of $15''.5$ averaged over the vertical and horizontal directions. The effective beam size after smoothing is $15''.8$.

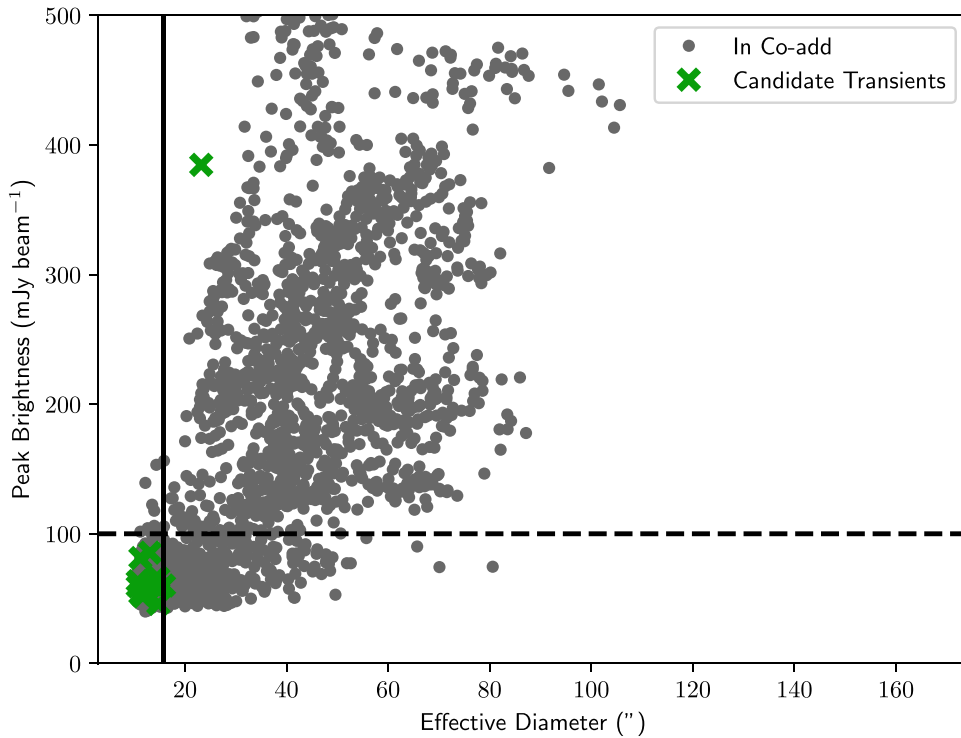


Figure 1. The 850 μm peak brightness vs. the effective diameter (assuming a circular projection) of all sources identified in all 19 OMC 2/3 epochs. Gray circles indicate sources identified in the coadd that are being analyzed by the current pipeline. Green X's indicate candidate transient sources that do not appear in the coadd (at the level of $5\sigma_{\text{rms}}$) but do appear in at least one epoch. A horizontal (dashed) line has been drawn at 100 mJy/beam $\sim 10\sigma_{\text{rms}}$. The vertical (solid) line represents the effective 850 μm beam FWHM after Gaussian smoothing.

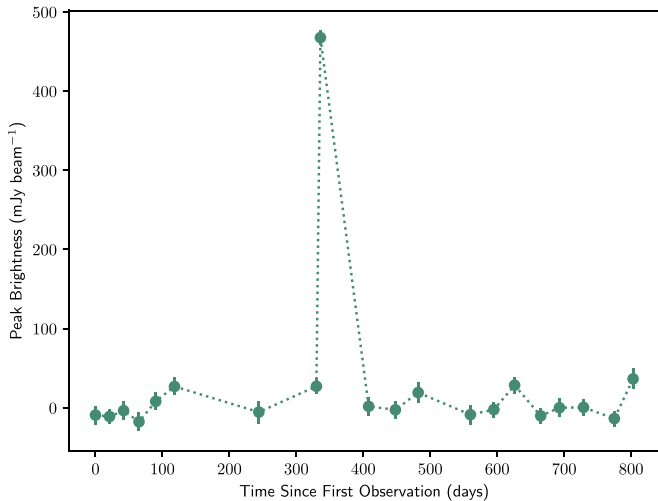


Figure 2. The 850 μm light curve of JW 566 over all observed epochs (see Table 1).

presents a light curve derived from extracting the value of the pixel at the peak location of JW 566.¹² The uncertainties are calculated by measuring the average pixel variance¹³ in a 20×20 pixel box centered on the source. Figure 3 shows that emission is not detected at this position in the previous image obtained six days earlier, or in the subsequent image obtained three months later. After coadding all 18 Transient Survey

¹² The small fluctuations are due to a slight amount of faint, extended emission in this region, which is better recovered in some epochs, but it is not associated with JW 566.

¹³ Each SCUBA-2 map has an associated “variance map” that records the variance of the bolometer signals contributing to each pixel.

epochs without a detection, the source is still not detected, with a noise of $\sigma_{\text{rms}} = 3 \text{ mJy beam}^{-1}$ in the coadded map (indicating an upper limit on the flux of $\sim 3\sigma_{\text{rms}} = 9 \text{ mJy beam}^{-1}$). The source is also not detected in the coadd of the SCUBA-2 images obtained by the JCMT Gould Belt Survey (Ward-Thompson et al. 2007) in 2011, with a sensitivity of $\sim 4 \text{ mJy beam}^{-1}$ (Data Release 3; Kirk et al. 2018).

The bright peak associated with JW 566 is detected in the map obtained during a 31 minute observation. The excess emission is consistent with an unresolved object at the (nonsmoothed) $14.''6$ resolution of the JCMT. The source is best detected in a residual map of the coadd (Figure 3(d)) subtracted from the flare epoch (Figure 3(b)) (after the images were rereduced with the new mask; see Section 2.2). The average brightness of the source during our observation is $466 \pm 47 \text{ mJy beam}^{-1}$ ($S/N = 48$), as measured by fitting a Gaussian profile to the source in the residual map.

4.2. Detecting the Flare at 450 μm

The brightness peak of JW 566 is also detected in the simultaneous 450 μm images obtained with SCUBA-2. The precipitable water vapor was low on the night of the flare, leading to a noise level of $\sigma_{\text{rms}} = 85 \text{ mJy beam}^{-1}$. Figure 4 presents the coadded data in image (a), excluding the 2016 November 26 epoch, the 2016 November 26 (flare) epoch in image (b), and a subtraction of image (a) from image (b) in image (c).

As in the case of the 850 μm observations, there is no indication of significant emission correlated with the position of JW 566 in any other SCUBA-2 image. A two-dimensional Gaussian profile fit to the residual 450 μm image yields a source peak of $500 \pm 107 \text{ mJy beam}^{-1}$ (the detection has an

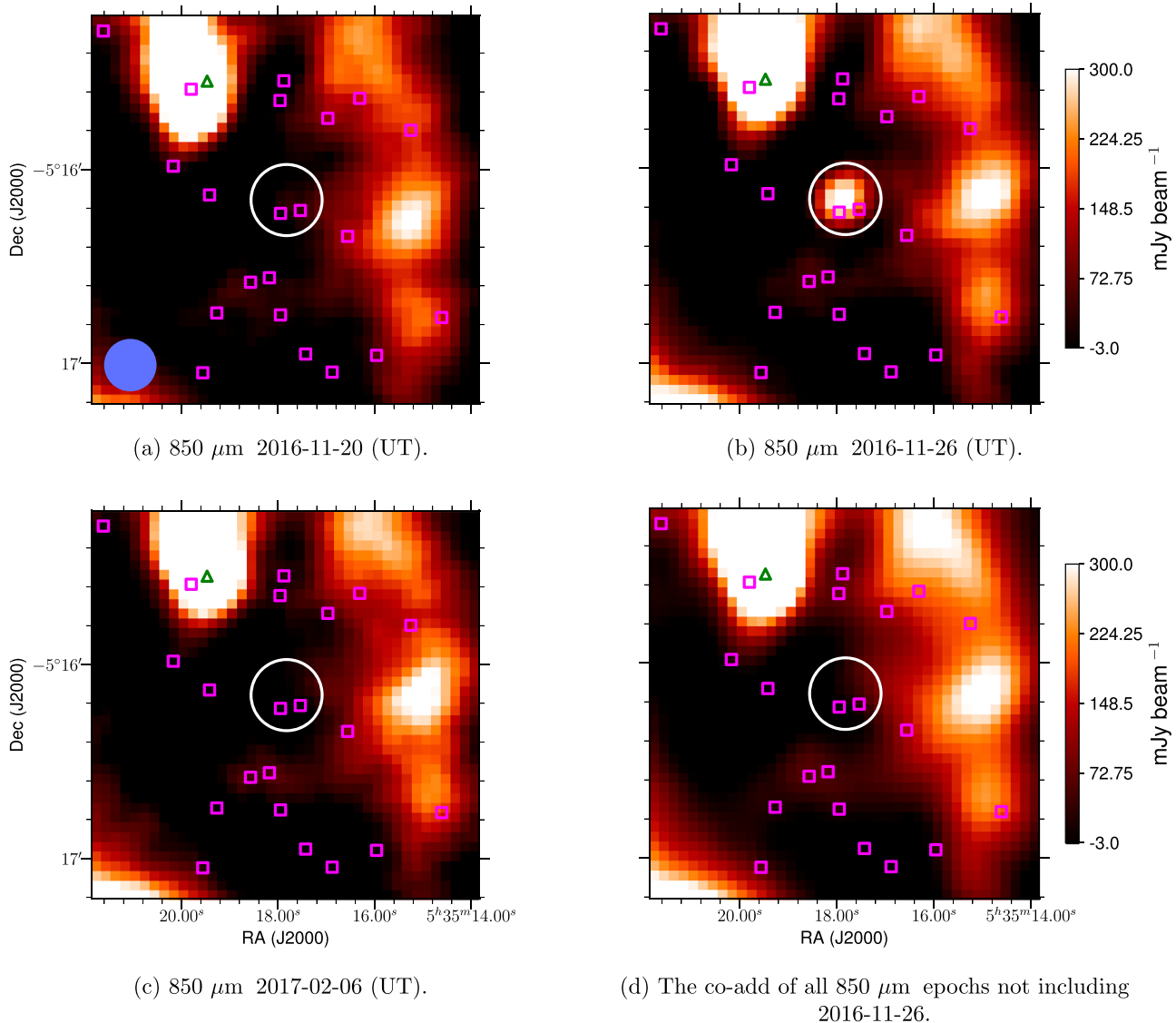


Figure 3. 850 μm observations of JW 566. Image (a) was observed as part of an engineering program carried out by JCMT staff on the night of 2016 November 20 (UT); the beam is shown in blue. Images (b) and (c) are two consecutive epochs taken as part of the JCMT Transient Survey; the flare occurred on 2016 November 26 (image (b)). The green triangle represents the position of a known protostar while the magenta squares mark the positions of known Class II YSOs (Megeath et al. 2012). The white circle shows the location of JW 566. Image (d) is a coadd of all 850 μm epochs not including 2016 November 26.

$S/N = 6$; see Section 2.2 for more information about the uncertainty).

4.3. Minute to Minute Variability at 850 μm

Since JW 566 is not detected in the engineering data, 6 days prior to the flare, the source must vary on timescales shorter than one week. In this section, we analyze the light curve of the bright emission peak in nine separate intervals within the 31.12 minute integration of 2016 November 26. In each interval, the source is detected with an S/N between 5 and 25 and is fit with a two-dimensional Gaussian profile to measure the source peak.

Figure 5 shows a dramatic decay in brightness during the 31 minute integration. The emission from JW 566 appears to already be in the dimming phase of the outburst, with an initial peak of 773 mJy beam^{-1} that drops to 400 mJy beam^{-1} by the end of the observation. The uncertainties for each measurement are calculated by measuring the square root average pixel variance in a 20×20 pixel box centered on the source.

To confirm that this brightness decrease is significant, we also analyze the light curves of five nonvarying unresolved sources with fluxes sampling the range of JW 566 in this epoch. Subdividing the raw time stream was performed in the same way individually for each source as it was for JW 566. Data points with abnormally high variances due to their proximity to the edge of the map or the uncertainty in surrounding, large-scale structure have been discarded. All of these sources are consistent with a constant flux during the 31 minute observation. The average standard deviation of the nonvarying sources is 9.7%. The light curve of JW 566 is monotonically decreasing and has a standard deviation of 23.2%, more than twice the average value of the nonvarying sources. At 450 μm , the noise is too high to perform a similar analysis.

5. Discussion

Young stars are known to undergo large, short-lived (timescales of hours to days) outbursts detectable at millimeter

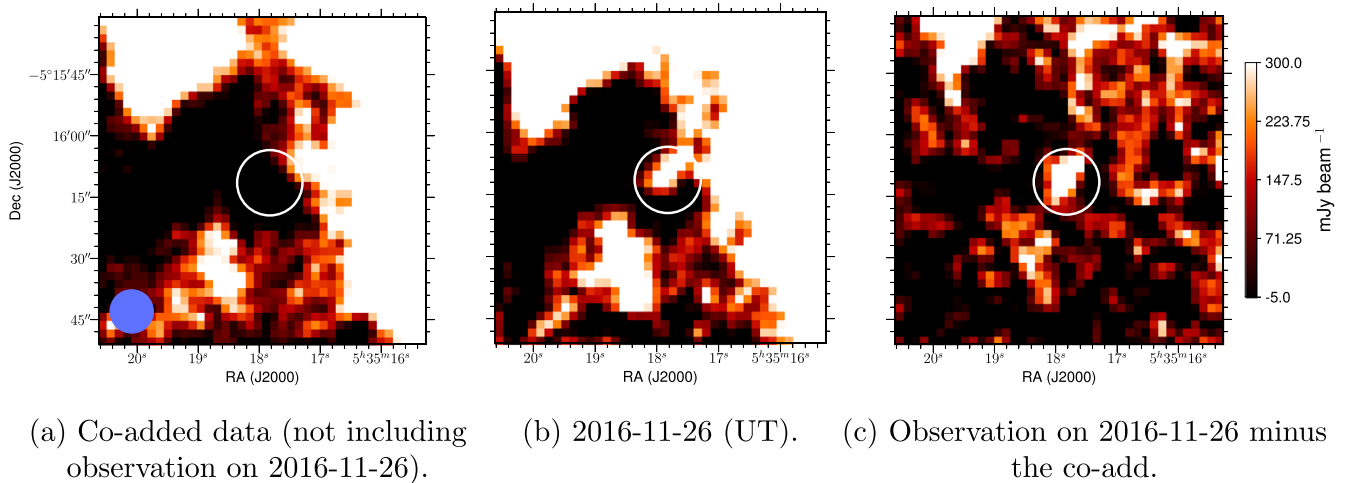


Figure 4. 450 μm observations of JW 566. The beam size is shown as a blue circle in image (a), the coadded data not including the 2016 November 26 epoch. Image (b) shows the 2016 November 26 epoch when the flare occurred. Image (c) shows the subtraction of image (a) from image (b). Compact structure is obvious in the residual.

and centimeter wavelengths (Bower et al. 2003; Furuya et al. 2003; Massi et al. 2006; Salter et al. 2010; Forbrich et al. 2017). Flare studies tend to focus on these frequencies, leaving the submillimeter frequency space of JCMT largely unexplored.

At a distance of 389 pc,¹⁴ the measured 850 μm flux (466 mJy beam^{-1}) corresponds to a radio luminosity of $L_\nu = 8 \times 10^{19} \text{ erg s}^{-1} \text{ Hz}^{-1}$. A natural comparison point for this result is with the 2003 outburst event of the T Tauri star GMR-A in the Orion Nebula (Bower et al. 2003; see also Furuya et al. 2003). GMR-A had a radio luminosity of $L_\nu = 3 \times 10^{19} \text{ erg s}^{-1} \text{ Hz}^{-1}$ at 86 GHz (assuming the same distance of 389 pc), which makes the JW 566 flare an order of magnitude brighter in terms of νL_ν . Salter et al. (2008) and Massi et al. (2006) observed flares associated with the DQ Tau binary system at 115 GHz and the V773 Tau quadruplet at 90 GHz, respectively, with radio luminosities of $\sim 6 \times 10^{19} \text{ erg s}^{-1} \text{ Hz}^{-1}$. If the flare associated with JW 566 follows the X-ray/radio luminosity correlation (see, for example, Güdel 2002), then it is 10 orders of magnitude brighter than a typical solar flare. It is plausible that this is the most luminous flare ever recorded in a young star. In the future, coordinated observations are required at 450, 850 μm , and other wavelengths to reveal the relationship between the fluxes at different energy regimes.

The OMC 2/3 field has been observed with SCUBA-2 for 10 hr since 2015 December 26, and this is the first significant flare event of its kind discovered in those data. In total, there are ~ 600 known (Spitzer identified; Megeath et al. 2012) Class II (disk) objects present in the field of view. Therefore, the current detection rate of flare events of this magnitude is $1/(600 \text{ stars} \times 10 \text{ hr}) \approx 1\text{--}2 \text{ yr}^{-1} \text{ star}^{-1}$. It is likely that there is a luminosity function for submillimeter flares that scales as a power law, $N \propto L^\beta$, where $\beta < 0$. More and deeper observations of this field, including seven additional hours from our Transient survey by 2020 February, will allow us to measure the flare rate over a wide range of luminosities. Additionally,

¹⁴ We adopt a distance of 389 pc to JW 566 due to its proximity with the Orion Nebula Cluster. This is based on the analysis of Kounkel et al. (2018), who used Very Long Baseline Array data (Kounkel et al. 2017) and GAIA DR2 astrometry (Gaia Collaboration et al. 2018).

we will be able to perform a more complete search by detecting fainter, longer timescale events by coadding subsets of the data.

The detection of a coronal flare at submillimeter wavelengths adds another source of uncertainty in the measurement of disk masses (e.g., Pascucci et al. 2016). While submillimeter emission from most sources is produced by the thermal dust continuum emission within the protoplanetary disks, any unexpected emission from sources thought to be diskless should be tested to evaluate whether flaring may explain the emission. Indeed, unresolved 1.3 mm continuum emission from Prox Cen was initially interpreted as an indication of a candidate disk (Anglada et al. 2017) but later traced to a stellar flare (MacGregor et al. 2018).

5.1. Previous Observations of JW 566

The JW 566 binary system ($0''.86$ projected separation) has a disk around at least one of the components (Megeath et al. 2012). Daemgen et al. (2012) detected accretion around the K7 primary star but not the M1.5 secondary star. High-resolution optical spectra of JW 566 are not available, so it is unknown whether one or both stars are spectroscopic binaries. Interactions between the magnetospheres of close binaries are thought to excite coronal flares in DQ Tau (Salter et al. 2010) and perhaps other young stars.

Previous X-ray and radio observations demonstrate coronal flares from JW 566, as expected for young low-mass stars. Kounkel et al. (2014) classify the source as variable at both 4.5 and 7.5 GHz. In addition, JW 566 is a known X-ray source (Gagne et al. 1995; Garmire et al. 2000; Feigelson et al. 2002; Getman et al. 2005), with variability on timescales of hours. The JW 566 binary is one of the most luminous X-ray sources, with $L_X = 10^{31} \text{ erg s}^{-1}$, for its mass range in the COUP X-ray monitoring survey of the Orion Nebula (Getman et al. 2005). The extreme brightness is caused by a combination of saturated X-ray emission, with $\log L_X/L_{\text{bol}} = -3$, and large radii as measured by Daemgen et al. (2012). The X-ray emission is harder than average but not extreme among the COUP sample.

The source is detected in a 3 mm continuum image obtained by ALMA on 2015 December 26 (Hacar et al. 2018; see Figure 6). The 3 mm flux is measured to be 0.6 mJy, yielding

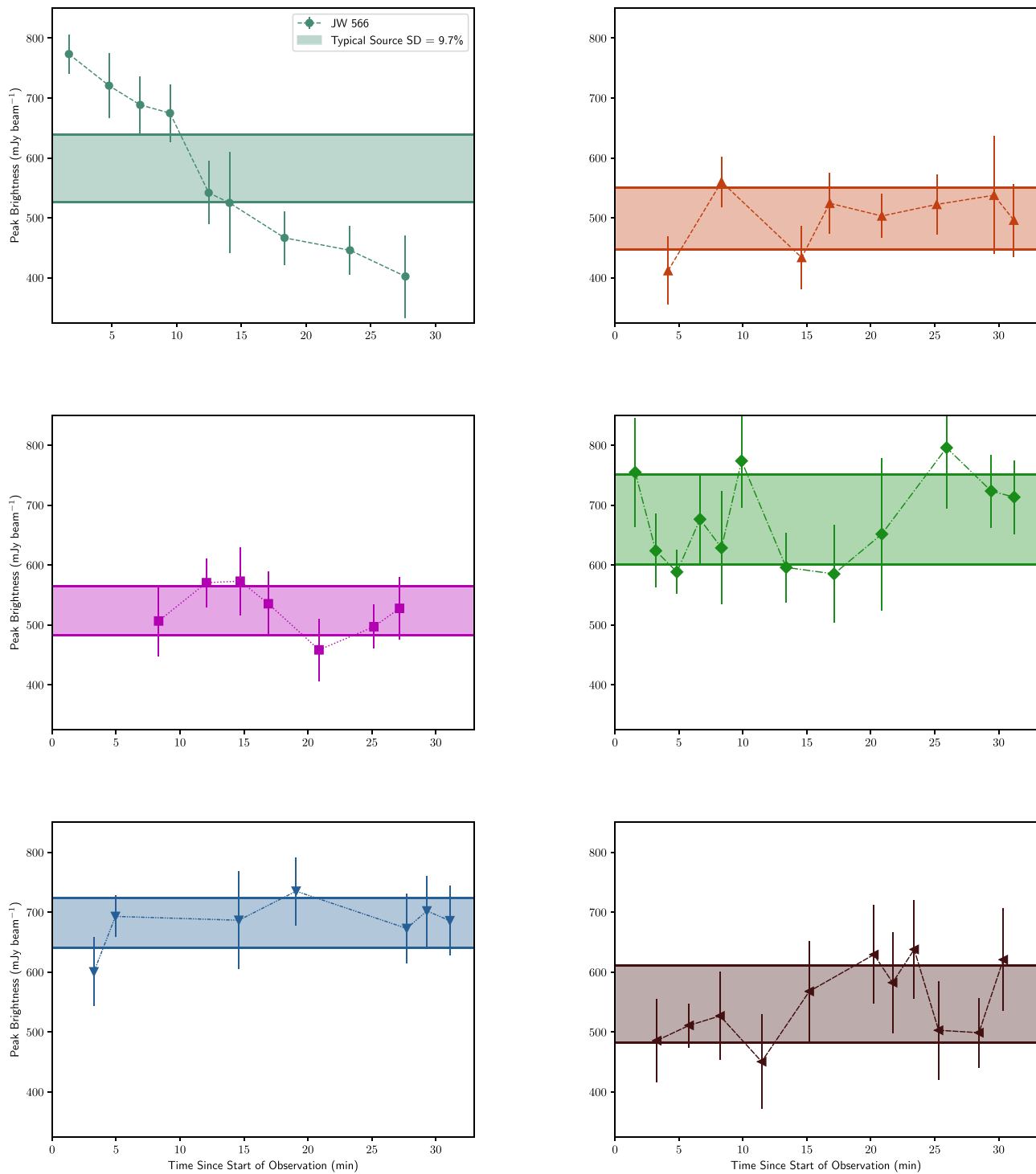


Figure 5. The $850\ \mu\text{m}$ peak brightness of JW 566 (top left) along with five typical sources in the brightness range displayed by JW 566 throughout the 31 minute integration. The sources were selected from different locations around the OMC 2/3 field. The light-curve standard deviations are shown by the shaded regions in each plot. The average standard deviation of the nonvarying sources (9.7%) is overlaid on JW 566’s light curve.

an S/N of 5.7. This presumably quiescent flux is a factor of 8×10^2 fainter than the $850\ \mu\text{m}$ continuum measurement of the flare, assuming a spectral index of 1. If the 3 mm flux is produced by the disk, a spectral index of ~ 2.3 (e.g., Ricci et al. 2010) would lead to an $850\ \mu\text{m}$ flux of $\sim 10\ \text{mJy beam}^{-1}$, very close to our current detection limit in the coadded image and within the flux range expected for disks in nearby star-forming regions (e.g., Ansdell et al. 2016; Pascucci et al. 2016).

Significant variability has not been detected at wavelengths other than millimeters and the X-rays, including in the optical, JHK_S (Ali & Depoy 1995; Tsujimoto et al. 2003; Skrutskie et al. 2006), at 3.6 and $4.5\ \mu\text{m}$ (Morales-Calderón et al. 2011), or in the far-IR (Billot et al. 2012). Unfortunately, we do not know of other available data at optical, infrared, or radio wavelengths at the time of this observation.

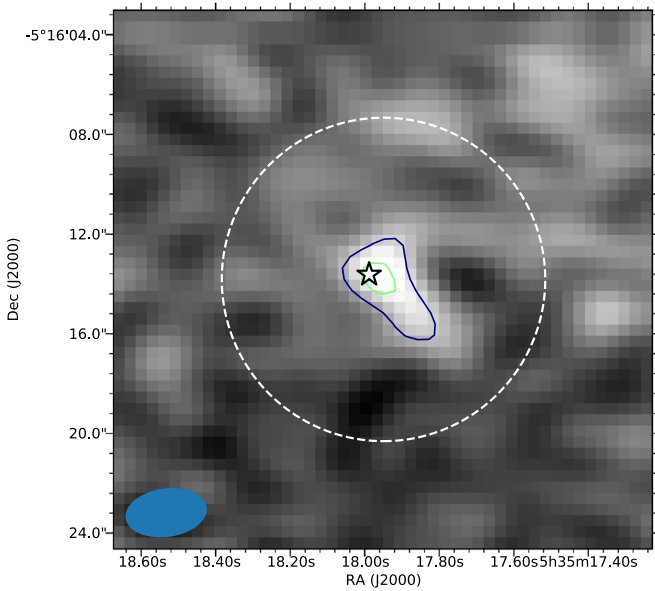


Figure 6. 3 mm continuum ALMA detection of JW 566 (star symbol). Contours are drawn at 3σ and 5σ . The dashed circle indicates the size of the SCUBA-2 $850\ \mu\text{m}$ beam FWHM. The beam is displayed in the lower left.

5.2. The Nature of JW 566's Flare

Based on the measured source fluxes at $450\ \mu\text{m}$ ($666\ \text{GHz}$, $f_{666} = 500 \pm 107\ \text{mJy beam}^{-1}$) and $850\ \mu\text{m}$ ($352\ \text{GHz}$, $f_{352} = 466 \pm 46.6\ \text{mJy beam}^{-1}$), we calculate a spectral index

$$\alpha = \frac{\left(\log(f_{666}) \pm \frac{\Delta f_{666}}{f_{666} \ln(10)}\right) - \left(\log(f_{352}) \pm \frac{\Delta f_{352}}{f_{352} \ln(10)}\right)}{\log(666\ \text{GHz}) - \log(352\ \text{GHz})}, \quad (1)$$

where Δf_ν represents the uncertainty in the fluxes, of $\alpha = 0.11 \pm 0.49$ over these wavelengths. While this value is consistent with nonthermal emission,¹⁵ the spectral index itself is not sufficient to discriminate the emission mechanism.

The brightness temperature, T_b can be approximated by

$$T_b \sim \left(\frac{1}{2k_B}\right) \times \lambda^2 \Delta S \times \left(\frac{D}{c\Delta t}\right)^2, \quad (2)$$

where k_B is Boltzmann's constant, ΔS is the change in flux over time Δt , λ is the wavelength, D is the distance to the source (389 pc), and c is the speed of light. The change in $850\ \mu\text{m}$ flux (ΔS) and its corresponding time frame (Δt) are derived from the light curve presented in Figure 5 with values of $373\ \text{mJy}$ ($\text{mJy} = \text{mJy beam}^{-1}$, for point sources) and $1661\ \text{s}$, respectively. This results in a brightness temperature of $T_b \sim 6 \times 10^4\ \text{K}$ and a light-crossing distance of $3.3\ \text{au}$. Constraining the angular scale to a stellar radius of $R_* = 2.5 R_\odot$ (the average radius of the two components in the JW 566 binary system; Daemgen et al. 2012) rather than $c\Delta t$, results in an estimate of the upper range of the brightness temperature of $T_b \sim 5 \times 10^9\ \text{K}$, though the origin of the flare could indeed be generated by a region smaller in scale than $R_* = 2.5 R_\odot$. With a projected separation of $335\ \text{au}$, it is very unlikely that an interbinary interaction is occurring among the

known components. These calculations strongly favor non-thermal emission. The most likely scenario is that the flare was caused by gyrosynchrotron/synchrotron radiation emitted by a reconnection event in the strong magnetic fields present in the corona of these young stars (see, e.g., Salter et al. 2010). This magnetic reconnection briefly energizes nonthermal particles, which appear as a flare. The detection of such an event at $850\ \mu\text{m}$ suggests a very-high-energy acceleration of electrons. Polarimetry data is required to separately constrain the contributions of gyrosynchrotron and synchrotron emission; such data, however, are not available for this event.

6. Summary

In this paper, we presented 450 and $850\ \mu\text{m}$ SCUBA-2 observations of a bright flare associated with the T Tauri binary system JW 566 (R.A., decl. = $5:35:17.94, -5:16:11$, J2000) obtained by the JCMT Transient Survey on 2016 November 26 (UT). The flare is measured to have a flux of $466 \pm 47\ \text{mJy beam}^{-1}$ at $850\ \mu\text{m}$ and $500 \pm 107\ \text{mJy beam}^{-1}$ at $450\ \mu\text{m}$ averaged over the observation (see Sections 4.1 and 4.2). We subdivided the 31 minute integration into nine intervals based on when the telescope scanned over the source and found a monotonic decrease of $337\ \text{mJy beam}^{-1}$ over $1661\ \text{s}$ (see Section 4.3). Constraining the size scale of the flare origin to the light-crossing time of our observation and to the stellar radius of one of the binary components results in a range of brightness temperatures between $T_b \sim 6 \times 10^4\ \text{K}$ and $T_b \sim 5 \times 10^9\ \text{K}$ (see Section 5.2). The flat spectral index, the short variability timescale, and a large T_b strongly indicate that the flare is a result of gyrosynchrotron/synchrotron emission, likely caused by a magnetic reconnection event.

The true timescale of the flare remains unknown, as there are no data available at other wavelengths during the time of our observation. The JCMT Transient Survey will continue through 2020 January, increasing the number of observations of the OMC 2/3 field by a factor of ~ 1.7 . Therefore, it is plausible that another burst of a similar magnitude will be detected. With new variable source detection methods (B. Lalchand et al. 2018, in preparation), we will be able to identify future events within $\sim 24\ \text{hr}$ of the data being taken by the telescope in order to perform follow-up observations.

The authors wish to extend their gratitude to Dr. David Berry for useful discussions regarding the $450\ \mu\text{m}$ data reduction, to Dr. Helen Kirk for assistance with the JCMT GBS DR3 observations, to Dr. Jenny Hatchell who provided comments that strengthened this work, and to the anonymous referee for insightful comments.

D.J. is supported by NRC Canada and an NSERC Discovery Grant. G.J.H. is supported by general grants 11473005 and 11773002 awarded by the National Science Foundation of China. J.E.L. is supported by the Basic Science Research Program through the National Research Foundation of Korea (grant No. NRF-2018R1A2B6003423) and the Korea Astronomy and Space Science Institute under the R&D program supervised by the Ministry of Science, ICT and Future Planning. A.H. is thankful for the support of the Netherlands Organisation for Scientific Research (NWO) under the VENI project 639.041.644. This paper makes use of the following ALMA data: ADS/JAO.ALMA#2015.1.00669.S.











¹⁵ Assuming a blackbody thermal spectrum, the temperature would need to be $4.9\ \text{K}$ to reproduce such a flat spectral index.

The authors wish to recognize and acknowledge the very significant cultural role and reverence that the summit of Maunakea has always had within the indigenous Hawaiian community. We are most fortunate to have the opportunity to conduct observations from this mountain. The James Clerk Maxwell Telescope is operated by the East Asian Observatory on behalf of The National Astronomical Observatory of Japan; Academia Sinica Institute of Astronomy and Astrophysics; the Korea Astronomy and Space Science Institute; the Operation, Maintenance and Upgrading Fund for Astronomical Telescopes and Facility Instruments, budgeted from the Ministry of Finance (MOF) of China and administrated by the Chinese Academy of Sciences (CAS), as well as the National Key R&D Program of China (No. 2017YFA0402700). Additional funding support is provided by the Science and Technology Facilities Council of the United Kingdom and participating universities in the United Kingdom and Canada. Additional funds for the construction of SCUBA-2 were provided by the Canada Foundation for Innovation. This research used the facilities of the Canadian Astronomy Data Centre operated by the National Research Council of Canada with the support of the Canadian Space Agency. This research has made use of the SIMBAD database, operated at CDS, Strasbourg, France (Wenger et al. 2000).

Facilities: JCMT, ALMA.

Software: astropy (Astropy Collaboration et al. 2013), matplotlib (Hunter 2007), aplpy (Robitaille & Bressert 2012) starlink (Currie et al. 2014),

ORCID iDs

Steve Mairs  <https://orcid.org/0000-0002-6956-0730>
 Bhavana Lalchand  <https://orcid.org/0000-0003-1618-2921>
 Geoffrey C. Bower  <https://orcid.org/0000-0003-4056-9982>
 Jan Forbrich  <https://orcid.org/0000-0001-8694-4966>
 Graham S. Bell  <https://orcid.org/0000-0003-0438-8228>
 Gregory J. Herczeg  <https://orcid.org/0000-0002-7154-6065>
 Doug Johnstone  <https://orcid.org/0000-0002-6773-459X>
 Wen-Ping Chen  <https://orcid.org/0000-0003-0262-272X>
 Jeong-Eun Lee  <https://orcid.org/0000-0003-3119-2087>
 Alvaro Hacar  <https://orcid.org/0000-0001-5397-6961>

References

- Ali, B., & Depoy, D. L. 1995, *AJ*, 109, 709
 Anglada, G., Amado, P. J., Ortiz, J. L., et al. 2017, *ApJL*, 850, L6
 Ansdell, M., Williams, J. P., van der Marel, N., et al. 2016, *ApJ*, 828, 46
 Astropy Collaboration, Robitaille, T. P., Tollerud, E. J., et al. 2013, *A&A*, 558, A33
 Benz, A. O., & Güdel, M. 2010, *ARA&A*, 48, 241
 Berry, D. S. 2015, *A&C*, 10, 22
 Billot, N., Morales-Calderón, M., Stauffer, J. R., Megeath, S. T., & Whitney, B. 2012, *ApJL*, 753, L35
 Bower, G. C., Plambeck, R. L., Bolatto, A., et al. 2003, *ApJ*, 598, 1140
 Buckle, J. V., Hills, R. E., Smith, H., et al. 2009, *MNRAS*, 399, 1026
 Chapin, E. L., Berry, D. S., Gibb, A. G., et al. 2013, *MNRAS*, 430, 2545
 Cleeves, L. I., Bergin, E. A., Öberg, K. I., et al. 2017, *ApJL*, 843, L3
 Coudé, S., Bastien, P., Kirk, H., et al. 2016, *MNRAS*, 457, 2139
 Currie, M. J., Berry, D. S., Jenness, T., et al. 2014, in ASP Conf. Ser. 485, *Astronomical Data Analysis Software and Systems XXIII*, ed. N. Manset & P. Forshay (San Francisco, CA: ASP), 391
 Daemgen, S., Correia, S., & Petr-Gotzens, M. G. 2012, *A&A*, 540, A46
 Dempsey, J. T., Friberg, P., Jenness, T., et al. 2013, *MNRAS*, 430, 2534
 Drabek, E., Hatchell, J., Friberg, P., et al. 2012, *MNRAS*, 426, 23
 Feigelson, E. D., Garmire, G. P., & Pravdo, S. H. 2002, *ApJ*, 572, 335
 Feigelson, E. D., & Montmerle, T. 1999, *ARA&A*, 37, 363
 Forbrich, J., Menten, K. M., & Reid, M. J. 2008, *A&A*, 477, 267
 Forbrich, J., Reid, M. J., Menten, K. M., et al. 2017, *ApJ*, 844, 109
 Forbrich, J., Rivilla, V. M., Menten, K. M., et al. 2016, *ApJ*, 822, 93
 Fraschetti, F., Drake, J. J., Cohen, O., & Garraffo, C. 2018, *ApJ*, 853, 112
 Furuya, R. S., Shinnaga, H., Nakanishi, K., Momose, M., & Saito, M. 2003, *PASJ*, 55, L83
 Gagne, M., Caillault, J.-P., & Stauffer, J. R. 1995, *ApJ*, 445, 280
 Gaia Collaboration, Brown, A. G. A., Vallenari, A., et al. 2018, arXiv:1804.09365
 Garmire, G., Feigelson, E. D., Broos, P., et al. 2000, *AJ*, 120, 1426
 Getman, K. V., Feigelson, E. D., Broos, P. S., Micela, G., & Garmire, G. P. 2008a, *ApJ*, 688, 418
 Getman, K. V., Feigelson, E. D., Grosso, N., et al. 2005, *ApJS*, 160, 353
 Getman, K. V., Feigelson, E. D., Micela, G., et al. 2008b, *ApJ*, 688, 437
 Gibb, A. G., Jenness, T., & Economou, F. 2013, PICARD: A Pipeline for Combining and Analyzing Reduced Data, Starlink User Note 265 (Hilo, HI: Joint Astronomy Centre)
 Glassgold, A. E., Najita, J., & Igea, J. 2004, *ApJ*, 615, 972
 Güdel, M. 2002, *ARA&A*, 40, 217
 Güdel, M., & Benz, A. O. 1993, *ApJL*, 405, L63
 Güdel, M., Dvorak, R., Erkaev, N., et al. 2014, *Protostars and Planets VI* (Tucson, AZ: University of Arizona Press)
 Hacar, A., Tafalla, M., Forbrich, J., et al. 2018, *A&A*, 610, A77
 Herczeg, G. J., Johnstone, D., Mairs, S., et al. 2017, *ApJ*, 849, 43
 Holland, W. S., Bintley, D., Chapin, E. L., et al. 2013, *MNRAS*, 430, 2513
 Hunter, J. D. 2007, *CSE*, 9, 90
 Jenness, T., Chapin, E. L., Berry, D. S., et al. 2013, SMURF: SubMillimeter User Reduction Facility, Astrophysics Source Code Library, ascl:1310.007
 Johnstone, D., Hendricks, B., Herczeg, G. J., & Bruderer, S. 2013, *ApJ*, 765, 133
 Johnstone, D., Herczeg, G. J., Mairs, S., et al. 2018, *ApJ*, 854, 31
 Jones, B. F., & Walker, M. F. 1988, *AJ*, 95, 1755
 Kackley, R., Scott, D., Chapin, E., & Friberg, P. 2010, *Proc. SPIE*, 7740, 1
 Kirk, H., Hatchell, J., Johnstone, D., et al. 2018, arXiv:1808.07952
 Kounkel, M., Covey, K., Suárez, G., et al. 2018, *AJ*, 156, 84
 Kounkel, M., Hartmann, L., Loinard, L., et al. 2014, *ApJ*, 790, 49
 Kounkel, M., Hartmann, L., Loinard, L., et al. 2017, *ApJ*, 834, 142
 Lammer, H., Zerkle, A. L., Gebauer, S., et al. 2018, *A&ARv*, 26, 2
 MacGregor, M. A., Weinberger, A. J., Wilner, D. J., Kowalski, A. F., & Cranmer, S. R. 2018, *ApJL*, 855, L2
 Mairs, S., Johnstone, D., Kirk, H., et al. 2015, *MNRAS*, 454, 2557
 Mairs, S., Johnstone, D., Kirk, H., et al. 2017a, *ApJ*, 849, 107
 Mairs, S., Lane, J., Johnstone, D., et al. 2017b, *ApJ*, 843, 55
 Massi, M., Forbrich, J., Menten, K. M., et al. 2006, *A&A*, 453, 959
 Megeath, S. T., Gutermuth, R., Muzerolle, J., et al. 2012, *AJ*, 144, 192
 Morales-Calderón, M., Stauffer, J. R., Hillenbrand, L. A., et al. 2011, *ApJ*, 733, 50
 Parsons, H., Dempsey, J. T., Thomas, H. S., et al. 2018, *ApJS*, 234, 22
 Pascucci, I., Testi, L., Herczeg, G. J., et al. 2016, *ApJ*, 831, 125
 Rab, C., Güdel, M., Padovani, M., et al. 2017, *A&A*, 603, A96
 Ricci, L., Testi, L., Natta, A., et al. 2010, *A&A*, 512, A15
 Robitaille, T., & Bressert, E. 2012, APLpy: Astronomical Plotting Library in Python, Astrophysics Source Code Library, ascl:1208.017
 Salter, D. M., Kóspál, Á., Getman, K. V., et al. 2010, *A&A*, 521, A32
 Salter, D. M., Hogerheijde, M. R., & Blake, G. A. 2008, *A&A*, 492, L21
 Shu, F. H., Shang, H., Glassgold, A. E., & Lee, T. 1997, *Sci*, 277, 1475
 Skrutskie, M. F., Cutri, R. M., Stiening, R., et al. 2006, *AJ*, 131, 1163
 Sossi, P. A., Moynier, F., Chaussidon, M., et al. 2017, *NatAs*, 1, 0055
 Tsujimoto, M., Koyama, K., Kobayashi, N., et al. 2003, *AJ*, 125, 1537
 Ward-Thompson, D., Di Francesco, J., Hatchell, J., et al. 2007, *PASP*, 119, 855
 Wenger, M., Ochsenbein, F., Egret, D., et al. 2000, *A&AS*, 143, 9
 Yoo, H., Lee, J.-E., Mairs, S., et al. 2017, *ApJ*, 849, 69